ELSEVIER

Polymer 43 (2002) 2729–2736

polymer

www.elsevier.com/locate/polymer

Enhancement of corrosion protection effect of poly(*o*-ethoxyaniline) via the formation of poly(*o*-ethoxyaniline)–clay nanocomposite materials

Jui-Ming Yeh[a,*], Chi-Lun Chen[a], Yen-Chen Chen[a], Chin-Yi Ma[a], Kueir-Rarn Lee[b], Yen Wei[c], Shuxi Li[c]

[a]*Department of Chemistry, Chung-Yuan Christian University, Chung Li 320, Taiwan, ROC*
[b]*Department of Chemical Engineering, Nanya Institute of Technology, Chung Li 320, Taiwan, ROC*
[c]*Department of Chemistry, Drexel University, Philadelphia, PA 19104, USA*

Received 9 July 2001; received in revised form 30 November 2001; accepted 7 December 2001

Abstract

A series of polymer–clay nanocomposite (PCN) materials that consisted of emeraldine base of poly(*o*-ethoxyaniline) (PEA) and layered montmorillonite (MMT) clay were prepared by effectively dispersing the inorganic MMT clay platelets in organic PEA matrix via in situ oxidative polymerization. Organic *o*-ethoxyaniline monomers were first intercalated into the interlayer regions of organophilic clay hosts and were followed by a one-step oxidative polymerization. The as-synthesized PCN materials were characterized by Fourier transform infrared (FTIR) spectroscopy, wide-angle X-ray diffraction (XRD) and transmission electron microscopy (TEM).

PCN materials at low clay loading up to 3 wt% in the form of coating (e.g. 0.5 wt%) on cold-rolled steel (CRS) were found to exhibit much superior corrosion inhibition effect as compared to those of the bulk PEA by performing a series of electrochemical measurements of corrosion potential, polarization resistance, corrosion current and impedance spectroscopy in 5 wt% aqueous NaCl electrolyte. Furthermore, it was found that a further increase of clay loading up to 3 wt% results in a slightly enhanced molecular barrier property of PCN materials. The molecular weights of PEA extracted from PCN materials and bulk PEA were determined by gel permeation chromatography (GPC) analysis with NMP as eluant. Effects of the material composition on the molecular barrier, thermal stability, electrical conductivity and optical properties of PEA along with a series of PCN materials, in the form of free-standing film, fine powder and solution, were also studied by molecular permeability measurements (GPA), thermogravimetric analysis (TGA), differential scanning calorimetry (DSC), four-point probe technique and UV–vis spectra. © 2002 Published by Elsevier Science Ltd.

Keywords: Nanocomposite; Aniline; Corrosion

1. Introduction

Recently, polymer–clay nanocomposite (PCN) materials have evoked intense research interests due to their unique characteristics creating potential commercial applications. Based on many published literatures, PCN materials were reported to boost the thermal [1], mechanical [2], molecular barrier [3] and flame retardant properties [4] of polymers at low clay loading. The historical development of the PCN materials can be traced back to 1990 based on the research work of polyamide–clay nanocomposite by Toyota's research group [5]. Subsequently, several polymer–clay hybrid nanocomposite material systems were developed by the dispersion of alkylammonium-exchanged forms of montmorillonites (MMTs) in nylon [5], poly(methyl methacrylate) (PMMA) [6], epoxy resin [7], polyimide [8], polystyrene [9], etc.

On the other hand, electrically conducting polymers have drawn much attraction since the discovery that the conductivity of polyacetylene achieves the metallic region upon doping by oxidizing or reducing agents. Some specific conducting polymers, e.g. polyaniline, polythiophene and polypyrrole, have been found to display interesting photoelectronic properties. In the past decade, the use of polyanilines as anticorrosion coatings had been explored as the potential candidate to replace the chromium-containing materials based on their increases of known adverse health and environmental concern [10–21]. Wei and coworkers [19–21] demonstrated the corrosion inhibition effect of polyaniline by performing a series of electrochemical measurements on either doped or undoped polyaniline-coated cold-rolled steel (CRS) under different conditions. Wessling [18] claimed that the full mechanism of the corrosion inhibition of polyaniline on steel consisted of a potential shift due to the noble metal properties as well as the redox catalytic properties of polyaniline resulting in the

* Corresponding author.

0032-3861/02/$ - see front matter © 2002 Published by Elsevier Science Ltd.
PII: S0032-3861(02)00005-8

formation of passive layer of metal oxide. However, polyaniline is intractable in common organic solvents because of the stiffness of its backbone, which results from its delocalized electronic structure. Many soluble derivatives of polyaniline were therefore synthesized by polymerization of ring or nitrogen-substituted aniline monomers and/or by copolymerization [22,23]. Poly(*o*-ethoxyaniline) (PEA), a ring-substituted polyaniline derivative, has attracted considerable attention due to its good solubility in common organic solvents. Furthermore, corrosion inhibition effect of PEA coatings on a variety of metallic surfaces has also been reported elsewhere [24].

Recently, PCNs that consisted of conductive polyaniline and different layered materials were found to display novel property, which can be observed from the interaction of the two dissimilar chemical components at the molecular level. There are a number of reports on the preparation and properties for nanocomposites of polyaniline and various layered materials [25–31]. We have found that the incorporation of nanolayers of MMT clay into polyaniline matrix led to an effectively enhanced corrosion inhibition of polyaniline on CRS based on a number of electrochemical corrosion measurements [34].

In this paper, we prepared a series of poly(*o*-ethoxyaniline)–clay nanocomposite (PCN) materials by effectively dispersing the inorganic nanolayers of MMT clay in organic PEA matrix via in situ oxidative polymerization. The as-synthesized PCN materials were characterized by infrared spectroscopy, wide-angle X-ray diffraction (XRD) and transmission electron microscopy (TEM). PCN materials at low clay loading in the form of coating (e.g. 0.5 wt%) on CRS were found to exhibit much superior corrosion inhibition effect as compared to those of the bulk PEA by performing a series of electrochemical measurements of corrosion potential, polarization resistance, corrosion current and impedance spectroscopy in 5 wt% aqueous NaCl electrolyte. The molecular weights of PEA extracted from PCN materials and bulk PEA were determined by gel permeation chromatography (GPC) analyses with NMP as eluant. Effects of the material composition on the molecular barrier, thermal stability, electrical conductivity and optical properties of PEA along with a series of PCN materials, in the form of free-standing film, fine powder and solution, were also studied by molecular permeability measurements, thermogravimetric analysis (TGA), four-point probe technique and UV–vis spectra.

2. Experimental

2.1. Chemicals and instrumentations

1-Methyl-2-pyrrolidinone (NMP) (99.97%, Tedia), tetradecyltrimethylammonium chloride (Fluka), lithium chloride (ACROS, 99%), methanol (Tedia, ACS grade), polysulfone (AMOCO, Udel P-3500, $M_w = 35{,}000$), ammonium peroxodisulfate (SHOWA) were used as received without further purification. *o*-Ethoxyaniline (99%, ACROS) was doubly distilled under a reduced pressure. Ammoniaque solution (25%, Riedel-de Haen) and hydrochloric acid (37%, Riedel-de Haen) were applied to prepare the 1.0 M NH_4OH and 1.0 M HCl aqueous solution. The used MMT clay consisted of a CEC value of 114 mequiv./100 g and a unit cell formula $Ca^{2+}_{0.084}{\cdot}Na^{+}_{0.143}[Al_{1.69}Mg_{0.31}]Si_4O_{10}(OH)_2{\cdot}2H_2O$ was provided by ITRI. Wide-angle powder XRD study of the samples was carried out by Rigaku D/MAX-3C OD-2988N X-ray diffractometer with copper target and Ni filter at a scanning rate of 4°/min. The samples for TEM study was first prepared by adding poly(*o*-ethoxyaniline)–clay powder into PMMA capsules and by curing the PMMA at 100 °C for 24 h in a vacuum oven. Then the cured PMMA containing PCN materials were microtomed with Reichert-jumg Ultracut-E into 60–90 nm thick slices. Subsequently, one layer of carbon about 10 nm thick was deposited on these slices on mesh 100 copper nets for TEM observations on a JEOL-200FX with an acceleration voltage of 120 kV. SEIKO thermal analysis system equipped with model TG/DTA 220 TGA was employed to perform the thermal analyses under air flow. The programmed heating rate was 20 °C/min in most of the cases.

The standard electrochemical measurements of PCN-coated CRS coupons were carried out by a radiometer VoltaLab 21 and VoltaLab 40 Potentiostat/Galvanostat in a standard corrosion cell equipped with two graphite rod counter electrodes and a saturated SCE as well as the working electrode. The molecular weight of polymer extracted from all samples as well as from bulk PEA was determined by GPC. Waters GPC model 2 II equipped with a model 590 programmable solvent delivery module, a differential refractometer detector and a Styragel HT column were employed to perform the GPC studies. Fourier transform infrared (FTIR) spectra were recorded from pressed KBr pellets using a BIO-RAD FTS-7 FTIR spectrometer. A Yanagimoto Co. Ltd gas permeability measuring apparatus (model GTR 10) was employed to perform the permeation experiment of water vapor. The UV–vis spectra of a very dilute solution of the polymer bases in NMP were recorded on a Hitachi U-2000 UV–vis spectrometer at room temperature. Conductivity measurements were made on a four-point probe connected to a Keithley 2400 voltmeter constant-current source system. The sample were in the form of compacted disk pellets 12.6 mm in diameter and ~1 mm thick. Three measurements were made on all the duplicate samples.

2.2. Preparation of PEA

In a typical procedure, 10 ml of doubly distilled PEA (0.100 mol) was dissolved in 600 ml of 1.0 M HCl and the mixture was precooled to ~0 °C in an ice bath. A solution (200 ml) of 5.6 g (0.025 mol) $(NH_4)_2S_2O_8$ in 1.0 M HCl was

added dropwise to the aniline solution over a period of 15 min with a vigorous magnetic stirring. After ~2 h, the precipitate was collected on a Buchner funnel. Upon drying under dynamic vacuum at room temperature, the HCl-doped PEA was obtained as a green powder. The HCl-doped PEA was subsequently converted to emeraldine base form of PEA by stirring ~3 g of the fine powder of emeraldine hydrochloride in an excess amount (500 ml) of 1.0 M ammonium hydroxide at room temperature for 3 h. Upon filtering and drying under dynamic vacuum for 48 h, the emeraldine base (EB) form of PEA was obtained as a blue powder.

2.3. Preparation of organophilic clay, PCN materials and recovery of polymers

The typical procedure to prepare organophilic clay, PCN materials and recovery of polymers followed our previous published results [34].

2.4. Preparation of coatings and electrochemical measurements

As a typical procedure to prepare sample-coated coupons for electrochemical measurements, the emeraldine base form of PEA and PCN materials fine powder were first dissolved in NMP to give typically 1 wt% solution. The solution was subsequently cast dropwise onto the CRS coupons (1 × 1 cm) followed by drying in air for 48 h under fume hood to give coatings of ca. ~20 μm in thickness. Coupons were then mounted to the working electrode so that only the coated side of the coupon was in direct contact with the electrolyte. The edges of the coupons were sealed with super fast epoxy cement (SPAR®). Electrochemical corrosion measurements were carried out at room temperature. The electrolyte was (5 wt%) aqueous NaCl solution. Open circuit potential (OCP) at the equilibrium state of the system was recorded as the corrosion potential (E_{corr} in V vs. SCE). Polarization resistance (R_p in Ω/cm^2) was measured by sweeping the applied potential from 20 mV below to 20 mV above the E_{corr} at a scan rate of 500 mV/min and recording the corresponding current change. R_p value was obtained from the slope of the potential–current plot. Corrosion current (I_{corr}) was determined by superimposing a straight line along the linear portion of cathodic or anodic curve and extrapolating it through E_{corr}. The corrosion rate (R_{corr}, in milli-inches per year (MPY)) was calculated from the following equation [32]

$$R_{corr}\ (\mathrm{MPY}) = [0.13 I_{corr}(\mathrm{EW})]/Ad$$

where EW is the equivalent weight (g/equiv.), A the area (cm^2) and d the density (g/cm^3).

VoltaLab model 40 Potentiostat/Galvanostat was employed to perform the a.c. impedance spectroscopy measurements. Voltamaster 4 (Ver. 2.0) supplied by Radiometer Copenhagen was employed as software. Impedance measurements were carried out in the frequency range of 100K–100 mHz. The working electrode was first maintained in the test environment for 30 min before the impedance run. This step served to put the electrode in a reproducible initial state and to make sure that no blistering occurred during the conditioning period. All experiments were operated at a laboratory temperature of 25 ± 1 °C. All raw data were repeated at least three times to ensure reproducibility and statistical significance.

2.4. Preparation of free-standing films and barrier property measurements

In order to enhance the mechanical strength of free-standing film of as-synthesized materials for molecular (H_2O) barrier property measurements under high pressure difference conditions, a commercial polysulfone with high molecular weight ($M_w = 35{,}000$) was blended into the casting solution for film formation. Typically, 0.02 g of PEA or PCN materials in base form blended with 0.2 g of commercialized polysulfone with high molecular weight was dissolved by magnetically stirring 10 ml NMP at room temperature for 6–8 h. The solution was cast onto a substrate (e.g. a microscope glass slide). The solvent was allowed to evaporate at 50 °C under the hood for 10–12 h. The sample-coated glass substrate was then immersed into the distilled water for 12 h to give the free-standing film (or called membrane) of PEA and PCN materials followed by drying under vacuum for 24 h. A Yanagimoto Co. Ltd gas permeability measuring apparatus (model GTR 10) was employed to perform the permeation experiment of water vapor. Permeation of water vapor was performed using the same apparatus as pervaporation, except that the feed solution was not in contact with the membrane. The set-up is shown in Fig. 1. The feed solution was vaporized first and subsequently permeated through the membrane with an effective area of ~10.2 cm^2. The permeation rate was determined by measuring weight of permeate.

3. Results and discussions

The base forms of PEA can be represented by the following general formula, where R = $-OC_2H_5$:

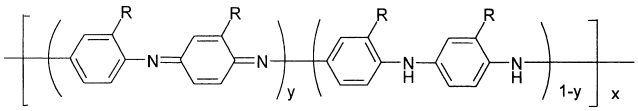

Here, y ranges from 1 for the fully oxidized polymer (so-called pernigraniline) to 0.5 for the half-oxidized polymer (emeraldine) and to 0 for the fully reduced polymer (leucoemeraldine). On the other hand, MMT is a clay mineral containing stacked silicate sheets measuring ~10 Å in thickness and ~2180 Å in length [33]. It possesses a high aspect ratio and a platey morphology. The chemical structures of MMT consist of two fused silica tetrahedral sheets sandwiching an edge-shared octahedral sheet of either

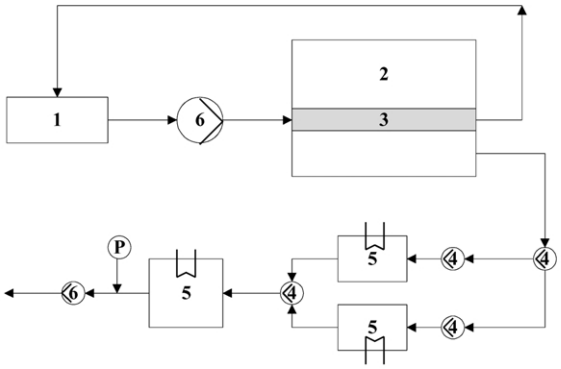

1: Feed. 2: Permeation cell.
3: Membrane. 4: Teflon cock.
5: Cooled trap. 6: Circulation pump.
7: Vacuum gauge.

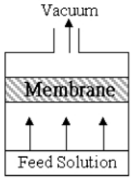

Fig. 1. Vapor permeation apparatus.

magnesium or aluminum hydroxide. The Na^+ and Ca^{2+} residing in the interlayer regions can be replaced by organic cations such as alkylammonium ions by a cationic-exchange reaction to render the hydrophilic layered silicate organophilic. MMT has a high swelling capacity, which is important for efficient intercalation of the polymer, and is composed of stacked silicate sheets that provide improved thermal stability, mechanical strength, fire retardant and molecular barrier properties.

To synthesize the PCN materials, organophilic clay was first prepared by a cation-exchange reaction between the sodium cations of MMT clay and alkylammonium ions of intercalating agent. Organic *o*-ethoxyaniline monomers were subsequently intercalated into the interlayer regions of organophilic clay hosts and followed by a one-step oxidative polymerization. The composition of the PCN materials was varied from 0 to 5 wt% of clay with respect to the PEA content as summarized in Table 1.

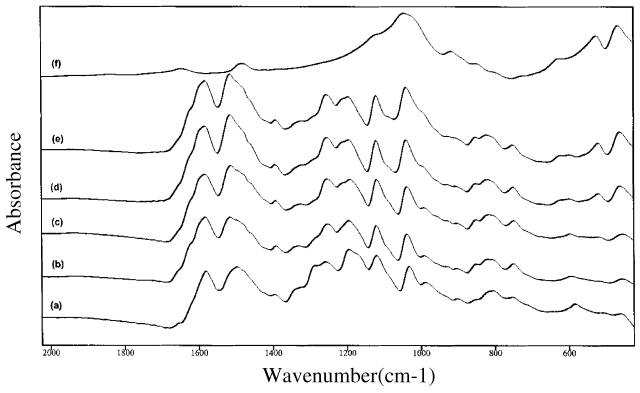

Fig. 2. FTIR spectra of (a) PEA, (b) CLEA0.5, (c) CLEA1, (d) CLEA3, (e) CLEA5, and (f) organophilic clay.

3.1. Characterization

The representative FTIR spectra of the organophilic clay, bulk PEA and PCN materials were given in Fig. 2. The characteristic vibration bands of PEA are at 1118 (C–O) and 1475 cm^{-1} (N–H), and those of MMT clay are shown at 1040 (Si–O), 600 (Al–O) and 420 cm^{-1} (Mg–O) [35]. As the loading of MMT clay is increased, the intensities of MMT clay bands become stronger in the FTIR spectra of PCN materials. Fig. 3 shows the wide-angle powder XRD patterns of organophilic clay and a series of PCN materials. In Fig. 3, the powder XRD patterns did not show any diffraction peak in $2\theta = 2$–10° as opposed to the diffraction peak at $2\theta = 4.75^\circ$ (d spacing = 1.86 nm) for organophilic clay, indicating the possibility of having exfoliated silicate layers of organophilic clay dispersed in PEA matrix. When the amount of organophilic clay increased to 3 wt%, there was a small peak appearing at $2\theta = 3.6$, corresponding to a d spacing of 2.45 nm. This implies that there is a small

Table 1
Relations of the composition of PEA–MMT clay nanocomposite materials with the E_{corr}, R_p, I_{corr} and R_{corr} measured from electrochemical methods (saturated calomel electrode was employed as reference electrode)

Compound code	Feed composition (wt%)		Inorganic content found in the product[a] (wt%)	Electrochemical corrosion measurement			
	PEA	MMT		E_{corr} (mV)	R_p (kΩ cm^2)	I_{corr} (μA/cm^2)	R_{corr} (MPY)
Bare	–	–	–	− 641.0	0.80	44.4	86.14
PEA	100	0	46.4	− 563.2	3.11	10.4	4.79
CLEA0.5	99.5	0.5	47.0	− 541.6	10.53	4.204	1.94
CLEA1	99	1	48.7	− 538.7	17.96	2.584	1.19
CLEA3	97	3	51.8	− 480.1	191.71	0.269	0.12
CLEA5	95	5	52.4	− 518.6	64.11	0.996	0.46

[a] As determined from TGA measurement.

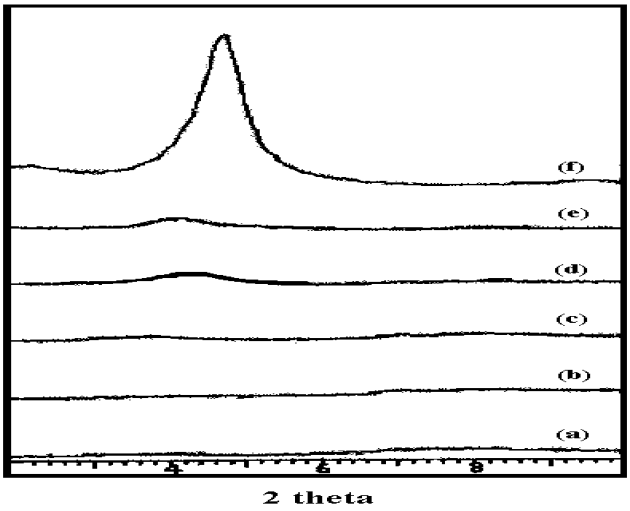

Fig. 3. Wide-angle powder XRD patterns of (a) PEA, (b) CLEA0.5, (c) CLEA1, (d) CLEA3, (e) CLEA5, and (f) organophilic clay.

amount of organophilic clay that cannot be exfoliated in the PEA and existed in the form of an intercalated layer structure.

In Fig. 4, the TEM of PCN materials with 3 wt% clay loading shows that the lamellar nanocomposite has a mixed nanomorphology. Individual silicate layers along with two, three and four layer stacks were found to be exfoliated in the PEA matrix. In addition, some larger intercalated tactoids can also be identified.

3.2. M_w and UV–vis spectra of extracted and bulk PEA

Molecular weights of the various polymer samples extracted from the nanolayers of MMT clays were obtained by GPC analyses. The polymer extracted from all samples as well as from bulk PEA were converted to the emeraldine base by treating with 1 M NH_4OH (aq.). The molecular weights of the NMP-soluble component displayed monomodal peak distributions corresponding to a molecular weight value, as shown in Table 2. The molecular weights of extracted PEA were found to be significantly lower than that of the bulk PEA, indicating the structurally restricted polymerization conditions in the intragallery region of the MMT clay [16,17]. For the optical property studies, it is interesting to find that the peak position of the exciton absorption is 620 nm for the CLEA3 in NMP solution, which is between 613 nm for the CLEA5 and 622 nm for

Table 2
Molecular weights of bulk and extracted PEA

Sample	$\bar{M}_w$	$\bar{M}_n$	Polydispersity
PEA	49,986	32,158	1.55
CLEA0.5	7020	5483	1.28
CLEA1	3325	2496	1.33
CLEA3	3187	2553	1.25
CLEA5	2315	1437	1.61

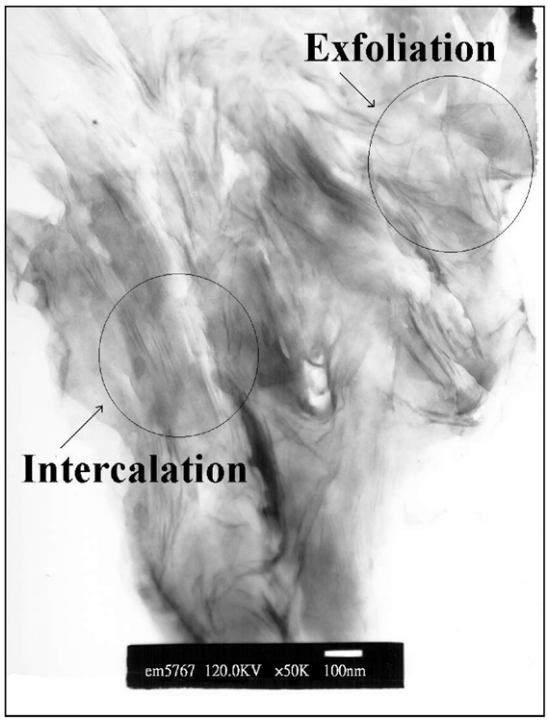

Fig. 4. TEM of CLEA3, with exfoliated and intercalated domains.

PEA in the same solvent as shown in Fig. 5. Although the ratio of the π–π^* transition intensity to the exciton transition intensity for the CLEA5 is about 1.60 compared to ~1.29 for PEA, it is understood that there are relatively fewer exciton units than π–π^* transition units in CLEA5 compared to PEA because of end group effects [38]. On the other hand, the UV–vis spectra of PCN materials displayed a blue shift compared to the bulk PEA material, reflecting a decreased conjugated chain length of PEA in PCN materials, which is consistent with the results obtained from GPC studies.

3.3. Corrosion inhibition properties of nanocomposite coatings

Corrosion inhibition effect of sample-coated CRS coupons can be observed from the values of corrosion potential (E_{corr}), polarization resistance (R_p), corrosion current (I_{corr}) and corrosion rate (R_{corr}), as shown in Table 1. The CRS coupon coated with emeraldine base of PEA shows a higher E_{corr} value than the uncoated CRS, which is consistent with previous observation [24]. However, it exhibited a lower E_{corr} value than the specimen coated with PCN materials. For example, the CLEA1-coated CRS displayed a high corrosion potential of ca. −538 mV at 30 min. Even after 5 h measurement, the potential remained at ca. −540 mV. Such E_{corr} value implies that the CLEA1-coated CRS is noble towards the electrochemical corrosion compared to the emeraldine base of PEA. The CLEA1-coated CRS showed a polarization resistance (R_p)

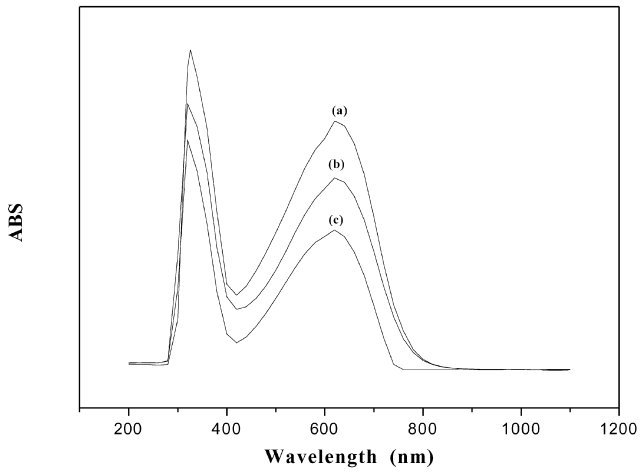

Fig. 5. UV–vis spectra of (a) PEA, (b) CLEA3, and (c) CLEA5.

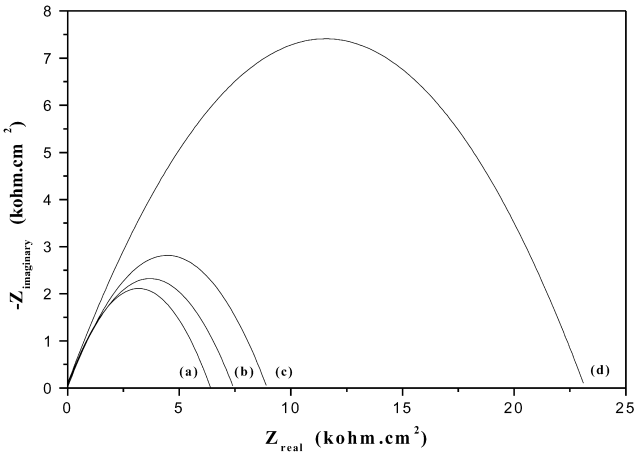

Fig. 7. Nyquist plots for (a) PEA-coated, (b) CLEA0.5-coated, (c) CLEA1-coated, (d) CLEA3-coated CRS, measured in 5 wt% aqueous NaCl solution.

value of $1.8 \times 10^4\ \Omega/cm^2$ in 5 wt% NaCl, which is about two orders of magnitude greater than the uncoated CRS. The Tafel plots for (a) uncoated, (b) PEA-coated, (c) CLEA1-coated and (d) CLEA3-coated are shown in Fig. 6. For example, the corrosion current (I_{corr}) of CLEA1-coated CRS is ca. 2.58 $\mu A/cm^2$, which is correspondent to a corrosion rate (R_{corr}) of ca. 1.19 MPY, as summarized in Table 1. Electrochemical corrosion current values of PCN materials as coatings on CRS were found to decrease gradually with further increase in clay loading up to 3 wt%. Electrochemical impedance spectroscopy (EIS) was also used to examine the activity difference between CRS surface after PEA and PCN material treatment. Four samples were prepared at the end. The first sample (a) was PEA-coated CRS. A series of samples denoted with (b)–(d) were coated by PCN materials with different clay loadings. The corrosion of these samples in 5 wt% aqueous NaCl electrolyte for 30 min was followed by EIS. Fig. 7 shows the Nyquist plots of the four samples. The charge transfer resistances of samples (a)–(d) as determined by the intersection of the low frequency end of the semicircle arc with the real axis are 6.4, 7.4, 8.9 and 23.1 $k\Omega\ cm^2$, respectively. The results clearly demonstrate that the sample, with the highest clay loading up to 3 wt%, has the greatest corrosion performance. EIS Bode plots (impedance vs. frequency) at various clay loadings of sample are shown in Fig. 8. The increase of impedance values at high clay loading in the low frequency region can be interpreted as the barrier effect of nanolayers of MMT dispersed in composites. Visual observation of the corrosion products clearly display that the PCN samples exhibiting corrosion protection have a grayish oxide layer form over the bare exposed CRS surface, similar to what was observed by Wessling [11–14] under the polyaniline dispersion coatings on steel. Therefore, in this study, we found that the corrosion protection of PCN materials on metallin surface might be resulted from both the redox catalytic property of PEA and barrier effect of MMT clay

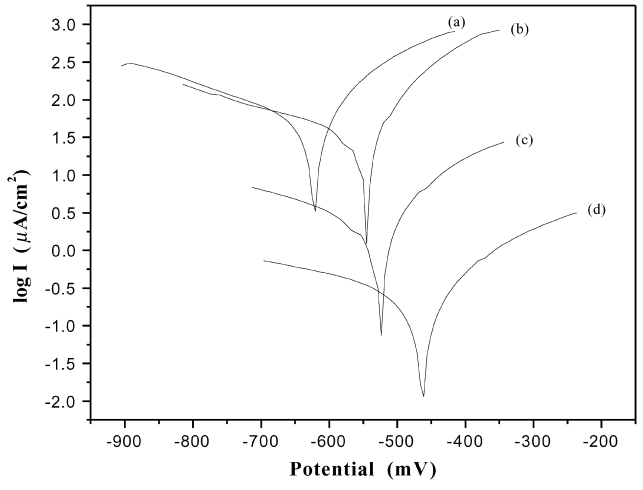

Fig. 6. Tafel plots for (a) uncoated, (b) PEA-coated, (c) CLEA1-coated, (d) CLEA3-coated CRS, measured in 5 wt% aqueous NaCl solution.

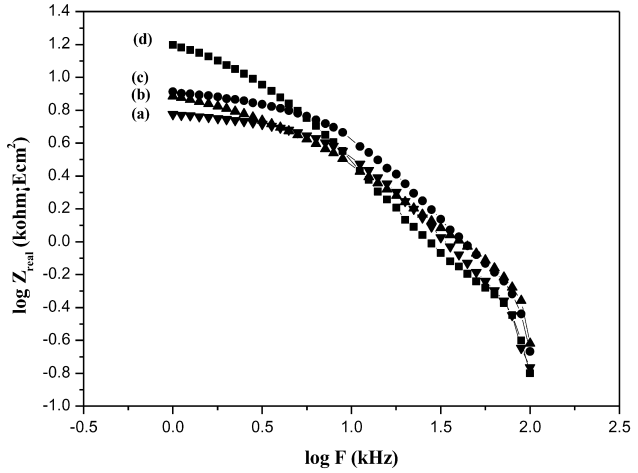

Fig. 8. Bode Plots for (a) PEA-coated, (b) CLEA0.5-coated, (c) CLEA1-coated, (d) CLEA3-coated CRS, measured in 5 wt% aqueous NaCl solution.

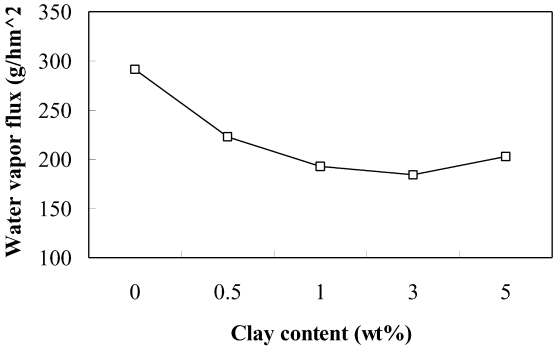

Fig. 9. Permeability of H_2O vapor as a function of the MMT clay content in the poly(*o*-ethoxyaniline)–clay nanocomposite materials.

platelets dispersing in composites. The barrier effect of PCN materials compared to bulk PEA might be resulted from dispersing silicate nanolayers of clay in PEA matrix to increase the tortousity of diffusion pathway of H_2O molecules [36]. This is further evidenced by the studies of the H_2O vapor barrier effect as discussed in Section 3.4.

3.4. Gas barrier of free-standing films (membranes) of nanocomposite materials

The free-standing film (or called membrane) of PCN materials and bulk PEA used for the molecular barrier measurements were prepared to have film thickness of ~40 μm. Compared to PEA, free-standing film of PCN materials at low clay loading (e.g. 0.5 wt%) shows about 23% reduction of H_2O permeability, as shown in Fig. 9. This is attributed to the barrier properties of the nanolayers of clay dispersed in the composite [8]. Furthermore, it should be noted that a further increase of clay loading up to 3 wt% results in a slightly enhanced molecular barrier property of bulk PCN materials. When the amount of clay loading increased to 5 wt%, there appeared an increased permeability of water vapor compared to PCN materials incorporating with 1 and 3 wt% clay, which might be attributed to the partial phase separation between the organic polymer and inorganic intercalated nanolayer of MMT clay.

3.5. Thermal properties and electrical conductivity of fine powders

Fig. 10 shows a typical TGA thermogram of weight loss as a function of temperature for PCN materials along with PEA, as measured under an air atmosphere. In general, there appeared to be several stages of weight loss starting at ~200 °C and ending at 650 °C, which might be corresponding to the degradation of intercalating agent followed by the structural decomposition of the polymers. Evidently, the onset of the thermal decomposition of those nanocomposites shifted significantly toward the higher temperature range than that of PEA, which confirms the enhancement of thermal stability of intercalated polymer [37]. After ~600 °C, all the curves became flat and mainly the

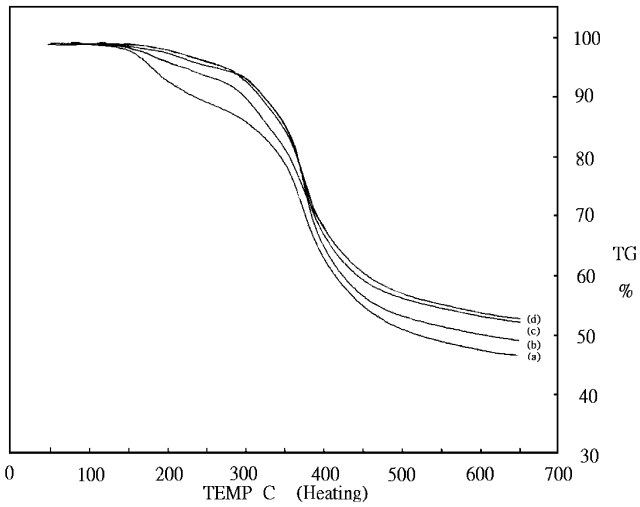

Fig. 10. TGA curves of (a) PEA, (b) CLEA1, (c) CLEA3, (d) CLEA5.

inorganic residue (i.e. Al_2O_3, MgO, SiO_2) remained. We found that the electrical conductivity of all the PCN materials was slightly smaller than that of bulk PEA, as shown in Fig. 11. This is expected because the MMT component is not electronically conductive and the incorporating of MMT clay into PEA matrix contributes to a lower molecular weight, reflecting a decreased electrical conductivity.

4. Concluding remarks

A series of nanocomposite materials that consisted of PEA and layered MMT clay were prepared by effectively dispersing the inorganic nanolayers of MMT clay in organic PEA matrix via in situ oxidative polymerization. As-synthesized materials were characterized by infrared spectroscopy, wide-angle powder XRD and TEM. Corrosion inhibition effect of PCN materials at low clay loading up to 3 wt%

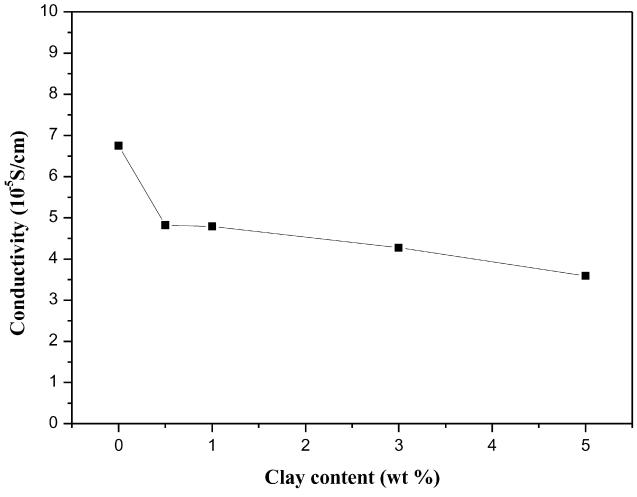

Fig. 11. Relationships between electrical conductivity and clay loading as obtained from four-probe technique measurements.

compared to emeraldine base of PEA was demonstrated by performing a series of electrochemical measurements of corrosion potential, polarization resistance, corrosion current and impedance spectroscopy on CRS in 5 wt% aqueous NaCl electrolyte. The coatings of PCN materials at low clay loading were found to show a better anticorrosion performance than the emeraldine base of PEA. The molecular weights of PEA extracted from lamellar PCN materials and bulk PEA were determined by GPC. The molecular weights of extracted PEA exhibited a decreased molecular weight compared to the bulk PEA, indicating the structurally restricted polymerization conditions in the intragallery region of the MMT clay. The effect of material composition on the molecular barrier, thermal stability, conductivity and optical properties of PEA along with a series of PCN materials in the form of free-standing film, fine powder and solution, were also studied by GPA and TGA, four-point probe technique and UV–vis spectra.

Acknowledgements

The financial support of this research by the NSC 89-2113-M-033-014 is gratefully acknowledged.

References

[1] Lan T, Kaviratna PD, Pinnavaia TJ. Chem Mater 1994;6:573.
[2] Tyan H-L, Liu Y-C, Wei K-H. Chem Mater 1999;11:1942.
[3] Wang Z, Pinnavaia TJ. Chem Mater 1998;10:3769.
[4] Gilman JW, Jackson CL, Morgan AB, Hayyis Jr. R, Manias E, Giannelis EP, Wuthenow M, Hilton D, Phillips SH. Chem Mater 2000;12:1866.
[5] Usuki A, Kawasumi M, Kojima Y, Okada A, Karauchi T, Kamigaito O. J Mater Res 1993;8:1774.
[6] Lee DC, Jang LW. J Appl Polym Sci 1996;61:1117.
[7] Lee DC, Jang LW. J Appl Polym Sci 1998;68:1997.
[8] Tyan H-L, Liu Y-C, Wei K-H. Chem Mater 1999;11:1942.
[9] Akelah A, Rehab A, Selim A, Agag T. J Mol Catal 1994;94:311.
[10] Deberry DW. J Electrochem Soc 1985;132:1027.
[11] Wessling B. Synth Met 1991:907 see also page 1057.
[12] Fahlman M, Jasty S, Epstein AJ. Synth Met 1997;85:1323.
[13] Ahmad N, MacDiarmid AG. Synth Met 1996;78:103.
[14] Talo A, Passiniemi P, Forsen O, Ylasaari S. Synth Met 1997;85:1333.
[15] Elsenbaumer RL, Lu WK, Wessling B. Int Conf Synth Met Seoul, Korea, Abstract No APL(POL)1–2; 1994.
[16] Wrobleski DA, Benicewicz BC, Thompson KG, Byran CJ. Polym Prepr (Am Chem Soc, Div Polym Chem) 1994;35(1):265.
[17] Li P, Tan TC, Lee JY. Synth Met 1997;88:237.
[18] Wessling B. Adv Mater 1994;6:226.
[19] Wei Y, Wang J, Jia X, Yeh J-M, Spellane P. Polymer 1995;36:4535.
[20] Camalet JL, Lacroix JC, Aeiyach S, Chane-Ching K, Lacaze PC. J Electroanal Chem 1996;416:179.
[21] Camalet JL, Lacroix JC, Aeiyach S, Lacaze PC. J Electroanal Chem 1998;445:117.
[22] Macinnes D, Funt BL. Synth Met 1988;25:235.
[23] Bergeron J-Y, Chevalier JW, Dao LH. J Chem Soc, Chem Commun 1990:180.
[24] Sathiyanarayanan S, Dhswan SK, Trivedi DC, Balakerishnan K. Corr Sci 1992;33(12):1831.
[25] Biswas M, Ray SS. J Appl Polym Sci 2000;77:2948.
[26] Wu C-G, DeGroot DC, Marcy HO, Schindler JL, Kannewurf CR, Liu Y-J, Hirpo W, Kanatzidis MG. Chem Mater 1996;8:1992.
[27] Wang L, Brazis P, Rocci M, Kannewurf CR, Kanatzidis MG. Chem Mater 1998;10:3298.
[28] Chao K-J, Ho S-Y, Chang T-C. US Patent 5,340,500; 1994.
[29] Giannelis E, Mehrota V. US Patent 5,032,547; 1991.
[30] Choi HJ, Kim JW, Kim SG, Kim BH, Joo J. Polym Mater Sci Engng 2000;82:245.
[31] Wu Q, Xue Z, Qi Z, Wang F. Polymer 2000;41:2029.
[32] Wei Y, Wang J, Jia X, Yeh J-M, Spellane P. Polym Mater Sci Engng 1995;72:563.
[33] Yano K, Usuki A, Okada A. J Polym Sci, Polym Chem Ed 1997;35:2289.
[34] Yeh J-M, Liou S-J, Lai C-Y, Wu P-C, Tsai T-Y. Chem Mater 2001;13:1131.
[35] Choi HJ, Kim JW, Kim SG, Kim BH, Joo J. Polym Mater Sci Engng 2000;82:245.
[36] Li P, Tan TC, Lee JY. Synth Met 1997;88:237.
[37] Lee DC, Jang LW. J Appl Polym Sci 1996;61:1117.
[38] Zhang WJ, Feng J, MacDiarmid AG, Epstein AJ. Synth Met 1997;84:119.